Searching for the oldest, most metal-poor stars in the SkyMapper Survey

Jennifer Walsh

under the direction of
Dr. Anna Frebel
Massachusetts Institute of Technology Department of Physics

Abstract

Finding stars with different metal abundances is very important for understanding the chemical evolution of the universe, which is the result of the nucleosynthesis of the elements within stars and supernova explosions. The most metal-poor stars are the oldest stars and thus provide information about the condition of the early universe. This research examined high-resolution spectra of 215 Galactic halo stars to determine the metallicity of each one. These stars were picked as candidate metal-poor stars using the SkyMapper telescope in Australia. Metallicity was measured by the ratio of iron (Fe) abundance to hydrogen (H) abundance in the star. 64 stars were found to have [Fe/H] < -2.0, which are stars with less than 1/100 of the solar Fe abundance. The metallicity distribution of the stars studied will help to improve future metal-poor candidate selections in the SkyMapper data. The most metal-poor stars in the sample show typical halo star α-abundances. These and future SkyMapper metal-poor stars will enable a more detailed understanding of the origin and evolution of chemical elements in the early universe.

Summary

Since the first stars were formed a few hundred million years after the Big Bang, there has been an evolution of element production. The first stars were formed from only hydrogen and helium. However, over time, the amount of elements heavier than those two has increased with each new generation of stars. This research examined absorption-line spectra of 215 stars in the Milky Way that possibly lack large amounts of elements heavier than hydrogen and helium. The ratio of iron, a heavier element, to hydrogen was determined for each star. Many stars were found that had an especially low ratio of iron to hydrogen compared to the young Sun. Additional study of this sample will be important for further understanding the first generations of stars and the creation of the chemical elements in the Universe.

1 Introduction

In the first minutes after the Big Bang, apart from traces of lithium, hydrogen and helium were the only elements that were present. Hydrogen consisted of ~ 0.75 of the matter by mass fraction, helium was ~ 0.25, and lithium was $\sim 2 \times 10^{-9}$. The first generation of stars, termed Population III stars, began to form a few hundred million years after the Big Bang. These stars were very massive - much more massive than typical stars observed today in the universe. Like all stars, the Population III stars performed nuclear fusion in their cores. Hydrogen atoms are fused to form helium, and helium atoms were subsequently fused to form carbon. α-elements, such as magnesium, calcium, and titanium, are made through helium capture by elements such as carbon and hence have atomic numbers that are multiples of four. Other fusion processes occured to create many additional elements. The large mass of these stars led them to expend their fuel faster and die earlier than smaller stars would. At the end of their lifetimes of a few million years, the Population III stars each entered into supernova, which is the stellar explosion that marks the death of a massive star. The type II supernovae explosions (SNII) of these stars chemically enriched the surrounding gas because, in this type of supernova, synthesis of new metals such as iron and α-elements occurs and the elements in the cores of the stars are released. Metals in astronomy include all elements that have larger atomic masses than helium. When the next generation of stars formed, they consequently contained not only hydrogen and helium but also traces of newly synthesized metals. As this process repeated, the abundances of metals in the universe and hence in the next generation stars increased. This entire phenomenon is called a chemical evolution because these supernovae gradually generated the elements that currently constitute the universe.

This particular type of supernova was the only method of generating new elements until about one billion years after the Big Bang. After this time, lower mass stars in binary systems

began to explode in supernovae type Ia and produce iron as well. Because of this chemical evolution, stars containing small amounts of metals tended to form at earlier times than stars that contain large amounts of metals. Thus, the lower abundances of heavy metals indirectly reveal an older age of a star. Some of these metal-poor stars, such as HE 1523, have been dated to as old as 13 billion years (Gyr) [1].

The metallicity of a star is its combined abundance of metals, which, in most cases for simplicity, is represented by [Fe/H], a measure of iron abundance compared to hydrogen abundance and taken in relation to the Sun. A star is considered metal-poor if it has less than 1/10 of the solar iron abundance. The Sun is only 4.6 Gyr and is a relatively young and metal-rich star. By definition, the Sun has [Fe/H] = 0. The definition of [Fe/H] is

$$[\text{Fe/H}] = \log(\text{Fe/H})_{star} - \log(\text{Fe/H})_{Sun}.$$

Stars preserve in their atmosphere the gas from which they were formed at birth. Stars can therefore serve as a a record of the chemical make-up of the universe from when they were born. Metal-poor stars, which are generally older than most stars, lead to further understanding of the chemical make-up of the early universe. Using stars as chemical records from different periods in the universe reveals the history of star formation and chemical evolution.

There have been two surveys in the past few decades that have led to the discovery of the most metal-poor stars known today. The calcium H and K line (HK) survey of Beers and colleagues [2, 3] was an objective-prism search. This method is the most efficient type for finding as many stars as possible. Stars from both the Northern and Southern Hemisphere skies were observed with low-resolution spectroscopy. The stars studied were generally classified into groups based on their metallicities (i.e. possibly metal-poor, very metal-poor, extremely metal-poor), which were estimated based on the observed strength of their ionized Ca II K

line at 3933 Å. This large-scale survey yielded approximately 1,000 Very Metal-Poor (VMP) stars with [Fe/H] < −2.0 and ∼ 100 Extremely Metal-Poor (EMP) stars with [Fe/H] < −3.0.

The second major survey was the Hamburg/ESO objective-prism survey (HES) [4]. This survey led to the discovery of additional metal-poor stars. The survey covered areas of the Southern sky that were not included in the HK survey. Stars in the Hamburg/ESO survey were examined with automatic spectral classification algorithms to measure strengths of Ca II K lines of several million objects surveyed. Again, line strengths were evaluated, and stars that had weak lines were classified as low-metallicity candidates. The most metal-poor stars known today were found in the HES. Frebel et al. ([5]) discovered the most iron-poor star currently known. The star, HE 1327−2326, has a metallicity of [Fe/H] = −5.4. This star and other metal-poor stars are believed to be part of the second generation of stars and therefore directly created from the remnants of the first stars.

2   Sample Selection and Observations

To learn about chemical evolution through nucleosynthesis in the cores and supernovae of stars, astronomers search for metal-poor stars. A new survey, the Southern Sky Survey, is observing stars with the 1.3m SkyMapper telescope. The telescope collects photometric data and is stationed at the Siding Spring Observatory in Australia. The Southern Sky Survey is an ongoing and long-term project that is surveying the entire Southern Sky. This survey has several science goals: to study the distribution of solar system objects beyond Neptune, nearby young stars, dark matter in the Galactic halo. The telescope is also undertaking a supernova survey that will discover ∼100 type Ia supernovae a year and collect information to understand the expansion history of the universe. Among one of the primary goals of the survey is also to find metal-poor stars and determine their metallicities [6].

At the SkyMapper telescope, several filters are available: the u, v, g, r, i, and z. The sky

is surveyed in the different filters, which only allows light with certain wavelengths to pass through. The calcium absorption line (Ca II K line) region around 3993 Å is observed with the narrow v filter. This way, metallicity information is gained by photometrically measuring the strength of the calcium absorption line. Measuring the difference between the stellar flux in the different filters (e.g. $g - r$) yields colors for each star. Detailed combination of colors involving the v filter and other colors enables the selection of low-metallicity candidates.

The candidate metal-poor stars were observed in Chile at the 6.5m Magellan-Clay telescope with the Magellan Inamori Kyocera Echelle (MIKE) spectrograph [7], which collects spectroscopic data. These spectroscopic data are necessary to determining the [Fe/H] of each star and to determine the chemical abundance pattern by analysis of the metal absorption lines of the spectra of each star. The nuclear fusion in the core of the star emits light, which is then absorbed by the atoms in the atmosphere of the star, causing an absorption line to appear in the spectrum. These absorption lines, depending on how strong they are, are evidence for the abundance of the element. Some example star spectra can be found in Figure 1. Their differing metallicities are based on the strength of the absorption lines.

We examined the spectra of 215 stars originally selected by the SkyMapper telescope and then observed by the Magellan-Clay telescope. The spectra were taken during three observing runs in November 2011, February 2012 and May 2012. Depending on weather conditions, either the 1.0" slit or the 0.7" slit was used, yielding a high spectral resolution of $R = \lambda/\Delta\lambda \sim 30,000$ and 35,000, respectively. The full principal wavelength range of the spectra is ~ 3500 to 9000 Å. Given that these spectra were taken in "snapshot" mode, only the region above ~ 5000 Å has sufficient signal-to-noise for a rough analysis of the [Fe/H] metallicity and a few other key elements. The spectra were reduced and wavelength calibrated at the telescope, but additional processing was required before beginning the analysis. The aim was then to determine the stellar metallicities and the metallicity distribution function of the combined sample and to further analyze the most metal-poor stars in the sample for
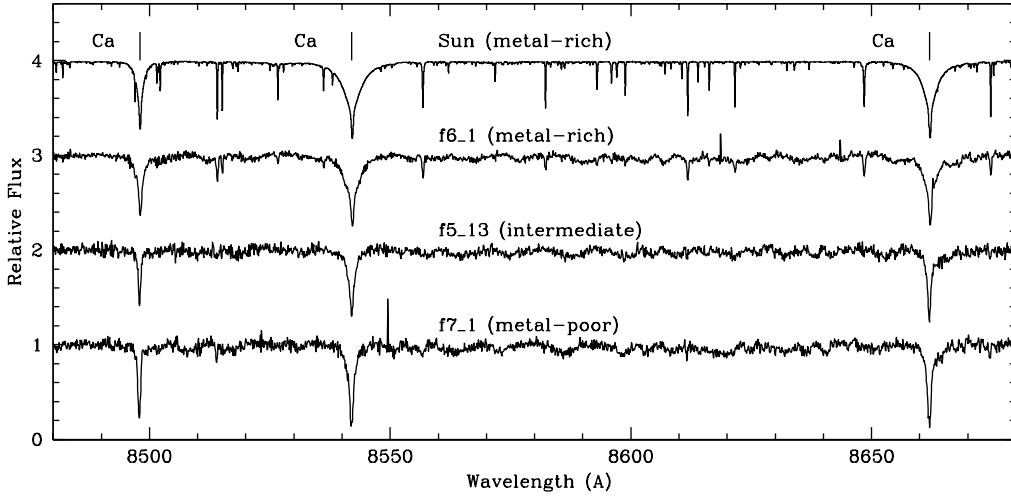
Figure 1: The spectra of four stars, the Sun, f6_1, f5_13, and f7_1.For each star, the calcium triplet lines are marked. All four of these stars contain calcium, but the difference in strength of the absorption lines reveal differences in metallicity. f3_16 is metal-poor, f5_9 has an intermediate metallicity, and f6_1 is metal-rich.

additional chemical abundances.

3   Methods

To find the metallicity of a particular star, its effective temperature, surface gravity, and microturbulence need to be determined. These three parameters characterize a star. Knowing these parameters enables the modeling of the atmosphere of the star. Together with measured equivalent widths of the absorption lines of the spectrum, abundances can then be calculated. The following steps had to be performed sequentially to use the information from the stellar spectra to calculate metallicity.

Several previously studied stars were also sent through this pipeline to gauge the accuracy of the iterative automanted abundance pipeline.

1. **Normalize the spectra.** The processed and reduced echelle spectra from the Magellan-Clay telescope for each star are high-resolution (0.7" slit $R = \lambda/\Delta\lambda \sim 30,000$ and 1.0" slit $R \sim 35,000$) line spectra. Each spectrum possess ~ 30 orders, which are small pieces of the spectrum. The wavelength range for these orders was 4950 to 9420 Å. To analyze the spectra, each bell-shaped order had to be normalized from a curve to a straight line to obtain flat orders. This normalization was done by fitting a line to the original curve in each order. The y-value of each point was then divided by the y-value of fitted line. The result is a new graph of absorption lines on a line with a normalized flux of 1. Normalized flux is merely a unitless measure of the relative intensity of light at a given wavelength in a spectrum. The final spectrum after normalization contained the merged orders.

2. **Correct radial velocity.** The spectra must be adjusted for the radial velocity of the star. The wavelength of photons being emitted from the star is subject to the Doppler effect because the star is moving with the Sun and the Earth. We can measure the motion (radial component) through the absorption line shift in the spectra. The velocity shift of the line is called radial velocity. The lines can be blue or red shifted, depending on whether they have moving toward or away from the Earth. Correction for radial velocity shifts the absorption lines in the spectrum of the star to their rest wavelengths. Examples of plots can be found in Figure 2. The velocity shift was determined by measurement of the wavelength difference between the position of the absorption lines in the stellar spectrum and their rest wavelengths.

3. **Estimate effective temperature ($\mathbf{T}_{eff}$).** The temperature of each star was estimated based on a visual inspection of the strength and slope of the Hα line. Nine stars whose temperatures were distinct from one another and well documented in the literature were used as a reference in estimating the temperature of every star. Figure
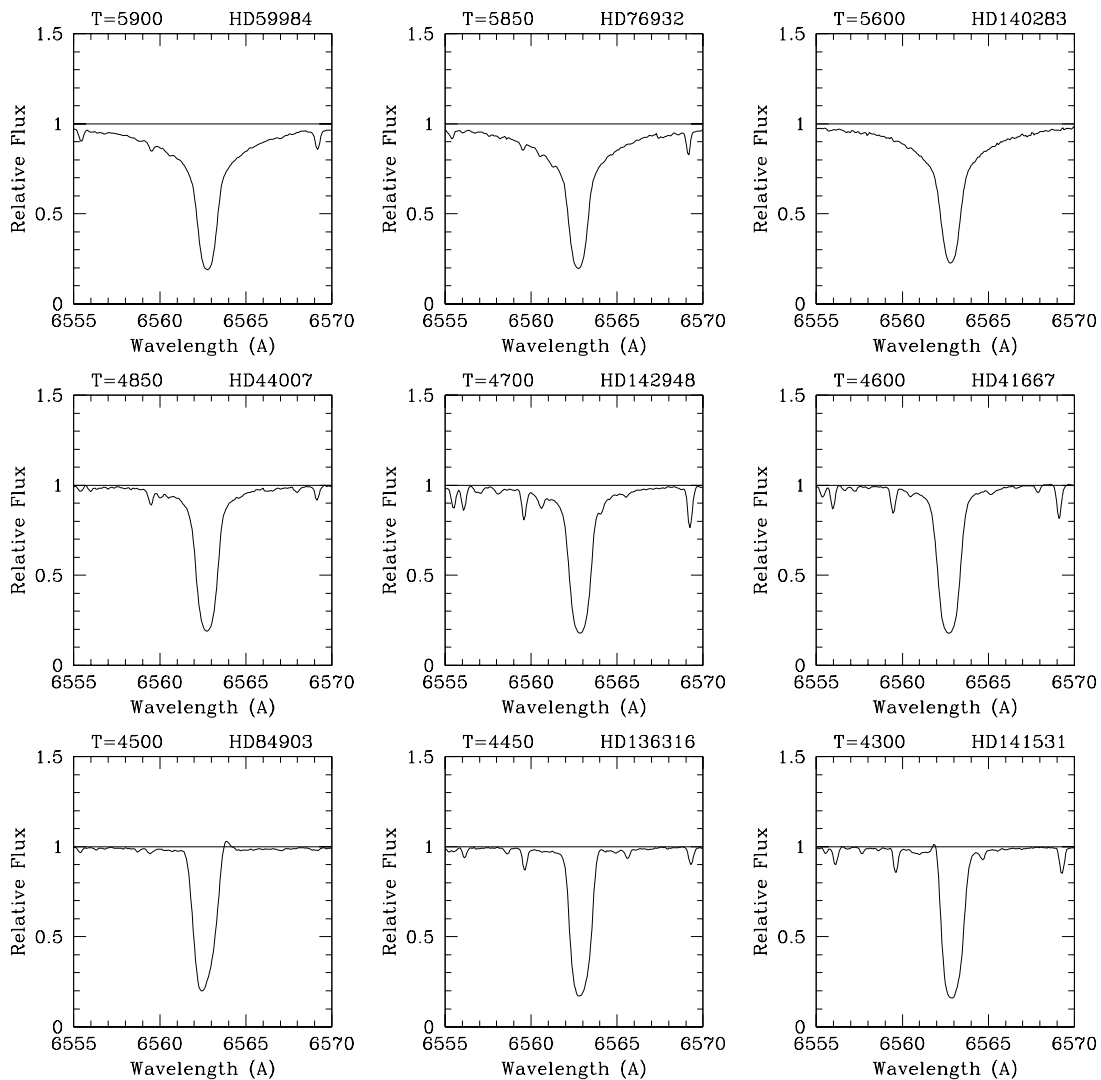
Figure 2: The Hα absorption lines of nine stars were used as references to estimate the temperatures of the stars in the sample. The Hα absorption line is found at 6562 Å. These temperatures for each reference star were chosen from literature curation. Wider absorption lines, lines whose tails extend far from the absorption line wavelength, suggest higher temperatures. Relative flux is the relative light intensity.

2 shows the Hα absorption line of each of the nine reference stars. The temperatures of these stars ranged from 4300 to 5900 K.The Hα lines of every star were then visually compared to the reference stars. As can be seen in Figure 2, higher temperatures cause

7

the Hα absorption line to be broader and therefore change the shapes of the line. Stars were considered close to the temperature of a given reference plot if the curve shape looked similar to the reference plot. Figure 3 shows the spectra and temperatures of some of the stars in the sample.
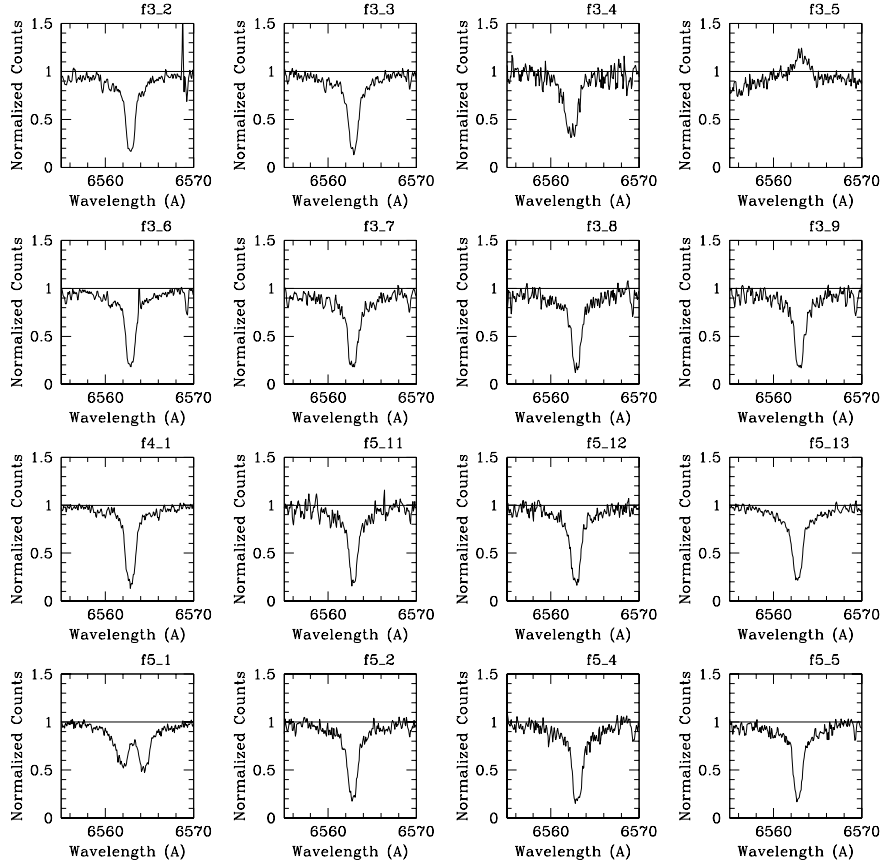
Figure 3: 16 stars whose temperatures were estimated based on the spectra in Figure 2.

4. **Estimate surface gravity ($\log g$).** The logarithm of the gravity was obtained using a theoretical Hertzsprung-Russell diagram. A conventional Hertzsprung-Russell diagram represents the path of the star throughout its life by plotting stellar luminosity versus the temperature or color. The theoretical diagram, which is based off the correlation between the luminosity and surface gravity, relates the log of gravity and temperature

8

of a particular star. Figure 4 shows T_{eff} versus $\log g$ for different metallicities and is based on stellar evolution and is called an isochrone. For a star with an estimated temperature, $\log g$ could be estimated by finding the $\log g$ value that fit on the isochrone at that temperature.
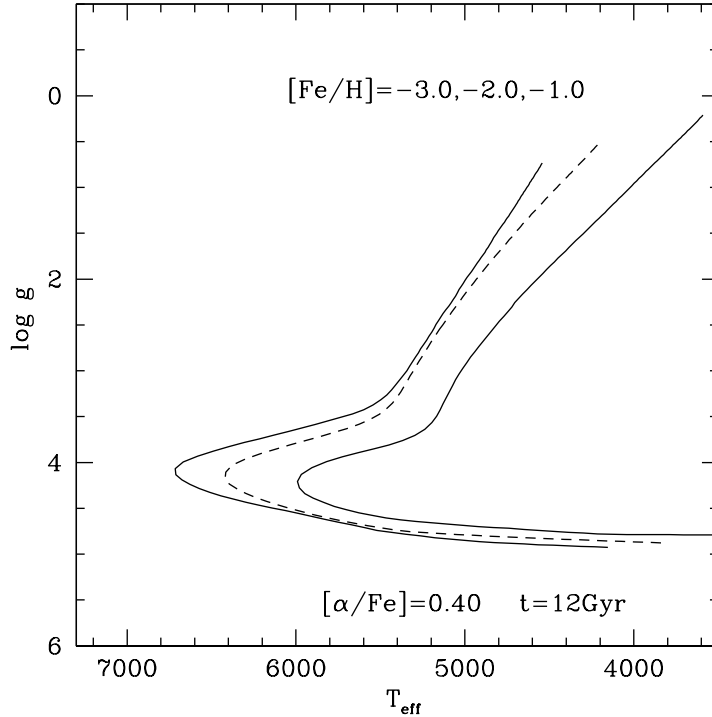
Figure 4: Modified Hertzsprung-Russell Diagram. Each star, according to its temperature, was assigned a $\log g$ value by the assumption that the temperature and gravity of the star was able to be plot on the line of the diagram.

5. **Measure equivalent width.** *Equivalent width* is the width of the rectangle that has an equal area and height to a single absorption line at its full width half maximum. Gaussian curves were used to fit the absorption lines and to determine the equivalent widths. The equivalent width increases with the strength of the absorption line. The stronger the absorption line that appears in the spectrum, the higher the abundance of

9

the element associated with that absorption line. In spectral analysis, large equivalent widths of metal absorption lines are, however, associated both with cool stars and with metal-rich stars. This degeneracy can be dealt with by determining first the temperature and then the metallicity of a star.

6. **Run pipeline and iterate.** The metallicity calculation is based on a linelist of absorption lines and the atomic physics properties of the star, corresponding equivalent width measurements for each absorption line, and a model atmosphere that imitates the outer atmosphere of the star where the absorption of the atoms of different elements occurs. These parameters were inputted into a newly developed, automated abundance pipeline to determine the metallicity. This pipline included the use of the computer program MOOG [8], which uses the model atmosphere of a star to determine the stellar abundances.

   (a) **Linelist:** A linelist includes the wavelength of the absorption line, the atomic number of the element that the line represents, the excitation potential for the transition that would create the absorption line, and the oscillation strength for that transition. This list is the basis for the automated equivalent width measurements.

      - *Excitation Potential* is the difference in potential between an excited atomic state and the ground state. If a photon with a particular energy hits an atom that has electrons with the correct excitation potential, the electron will absorb that energy and move up to a higher energy level. The excitation potential is different for each atomic level for each element. Often, lower excitation potential results in a stronger absorption line.
      - *Oscillator Strength* measures the strength of the transition an atom has when it has absorbed a photon. This quantity determines how strongly the transi-

tion is represented in an absorption line. Large oscillator strength will result in a strong absorption line.

(b) **Model Atmosphere:** The model atmosphere of a star is based on its effective temperature, surface gravity, microturbulence, metallicity, and $[\alpha/\text{Fe}]$ abundance ratio. Metallicity, for the purposes of the first iteration, was set first to $[\text{Fe/H}] = -2.5$ as an initial guess. After every iteration, the metallicity is adjusted based on the estimated abundances from the last iteration. The $[\alpha/\text{Fe}]$ ratio is the abundance of α-elements (e.g. magnesium, calcium, and titanium,) divided by the abundance of iron in the star. This parameter was not changed in iterating the program. Lastly, microturbulence is a model parameter that ensures that weak lines yield the same abundance as strong lines. Otherwise, the difference in equivalent width between weak and strong lines would lead to unphysical, different abundance measurements within a given star. Although this value varies for every star, the microturbulence has an effect only on the strong lines in a spectrum.

7. **Output.** The output is an equivalent width for each absorption line in the spectrum and abundances that result from the equivalent width. The equivalent widths are measured only once, but after each iteration, the output suggests ways to change the microturbulence, temperature, and $\log g$ values to obtain more accurate and precise stellar parameters.

Two graphs that demonstrate the parameter estimates are created for every star by the pipeline. The first graph is the plot of the Fe I absorption line abundance vs. their excitation potential. The second graph has Fe I line abundances plotted vs. $\log RW$. $\log RW$ relates the equivalent width (EW) and wavelength (λ) of a given absorption line. It is equal to $\log(EW/\lambda)$, with EW representing equivalent width for the given λ. The temperature and $\log g$ were modified between iterations based on the abundance

vs. excitaion potential graphs. A higher excitation potential for an absorption line reflects the weak strength of the line. In contrast, a larger $\log RW$ corresponds to stronger absorption lines.To obtain the final temperature, the line abundances were fit: no slope should be there for the true temperature of the star. The same was done for the microturbulence. A positive slope in the temperature plot suggested that the previously estimated temperature was too low, and vice versa for a negative slope. $\log g$ was adjusted according to the temperature adjustment made from analysis of this graph.

The abundances are gathered from every absorption line in the spectrum for a given element. The average of these line abundances is the final abundance of iron in the star. The abundances of the Sun are subtracted to arrive at an [Fe/H] value.

The final [Fe/H] values for every star in the sample, obtained from the iterative automative abundance pipeline, can be found in Appendix 1.

4   Results

The aim was to determine the metallicity of all the sample stars and to identify the most metal-poor stars in the sample. The metallicity distribution function (MDF) can then be used to improve on the photometric selection of metal-poor candidate stars.

4.1   Temperature Distribution

Figure 5 shows a histogram of the final effective temperatures of the sample. Main sequence stars are found between 5500 and 6500 K, and giants are between 5500 and 4500 K. The sample contains slightly more giants than main sequence stars. The gap between the two groups results from the sub-giant branch, which is a short evolutionary phase, so fewer star are expected
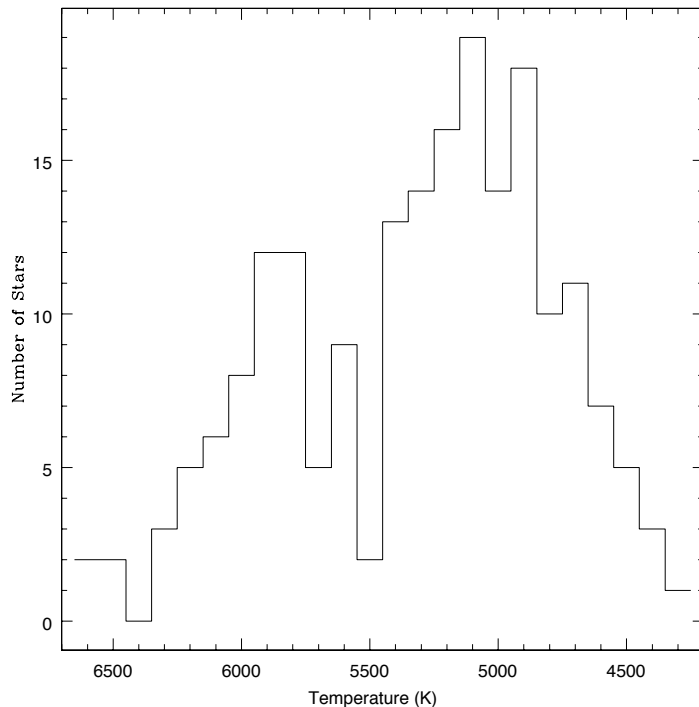
Figure 5: Temperature distribution in the sample.

4.2   The Most Metal-Poor Stars and the Metallicity Distribution

A primary goal of analyzing a large sample was to obtain a clear metallicity distribution function for the metal-poor candidate selections by the SkyMapper telescope. 64 stars with [Fe/H] values below -2.0 were found. Table 1 shows the [Fe/H] values of each of these stars.

Figure 6 shows the distribution of the metallicity values found of the entire sample. The outer and inner halo peaks are marked. The metallicity peak of this sample is at approximately [Fe/H]$= -1.8$.

Those stars will be re-observed with the Magellan telescope to obtain spectra with higher signa-to-noise. They will then be analyzed in great detail to measure ~ 15 elemental abundances. As a preliminary analysis, [Mg/Fe], [Ca/Fe] and [Ti/Fe] abundances were obtained for the most metal-poor stars with [Fe/H] < -2.5 in the sample. The pipeline was used

13
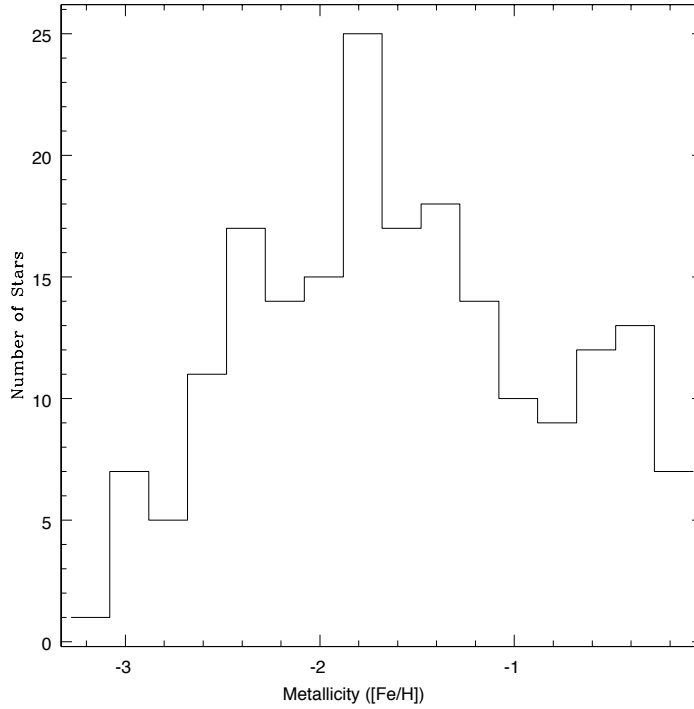
Figure 6: Histogram of the metallicity distribution of the sample. 64 stars have $[Fe/H] < -2.0$.

to measure the equivalent widths of the Mg, Ca and Ti absorption lines in the spectrum. Together with the stellar parameters the abundance could be calculated with MOOG. The results are shown in Figure 7 in comparison with stars from the literature **??**. As can be seen, the new SkyMapper stars follow the abundance trends of other halo stars. Their [Mg/Fe], [Ca/Fe] and [Ti/Fe] abundance of about 0.4 dex suggest that the new stars are also typical halo stars because these abundance ratios are reflective of chemical enrichment by Type II supernova in the early universe.

4.3 Standard Stars

Previously studied are referred to as the standard stars. We also run one particular star, HD74000, through the automtated iterative abundance pipeline to test the accuracy of the
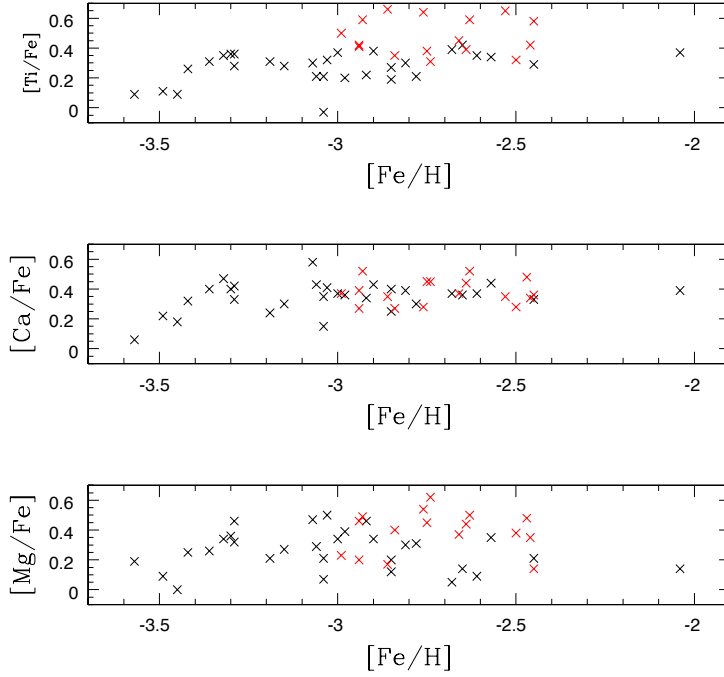
Figure 7: α-element abundances for the stars with $[Fe/H] < -2.5$.

pipeline. The stellar parameters of these stars were already known from the literature. The values calculated in this pipeine were compared to the parameters set forth by the litera-ture. Table 2 shows a comparison of the calculated stellar parameters of HD74000 with the parameters found on the SAO/NASA Astrophysics Data System (ADS).

Stellar parameters presented by Fulbright [9] and Cenarro et al. [10] for HD 74000 com-pared to the stellar parameters calculated by the automated iterative abundance pipeline. This pipeline was quite successful in determining the T_{eff}, $\log g$, and $[Fe/H]$ of the star, and will enable future analyses of thousands of stars.

Star Name	[Fe/H]
997-15-614	−2.50
1163-4-1120	−2.51
1163-6-1332	−2.54
f280	−2.54
f6-9	−2.58
1294-6-668	−2.60
f7-1	−2.64
f09-384	−2.66
f04-338	−2.67
2127-24-1381	−2.75
f6-9	−2.79
f09-80	−2.80
f6-7	−2.91
f02-339	−2.93
f3-12	−2.96
f6-8	−2.96
f03-68	−2.97
f33-0825-97	−3.00
f3-16	−3.18

Table 1: The [Fe/H] values of each star with [Fe/H]< −2.5. The stars are sorted by least to greatest metallicity. A full table of these values for every star in the sample can be found in Appendix 1.

Source	T_{eff}	$\log g$	[Fe/H]
This study	6100	3.9	−2.18
2000 Fulbright ([9])	6025	4.1	−2.08
2007 Cenarro et al. ([10])	6166	4.19	−2.02

Table 2: Standard star abundance comparison.

5   Discussion

The metallicity distribution of this set of stars has many significant implications. First, the distribution can improve the candidate metal-poor star selection process for the SkyMapper telescope. This selection process was designed to find stars of [Fe/H] < −2.0. As shown in Table 1, 64 stars with [Fe/H] < −2.0 were found, but, as shown in Figure 5, there were also

many stars that ultimately had higher metallicities. The stars in the high-metallicity peak can be compared to the colors found for each star by SkyMapper. This correlation between the metallicities and colors can be used in the future as a reference and a model for creating more stringent metal-poor searching methods at the SkyMapper telescope. The metallicity distribution shows that SkyMapper was able to find relatively metal-poor stars, even though many of the candidates failed to be metal-poor enough.

The average metallicity of the outer halo, as determined by [11], is [Fe/H]$= -2.2$, and the average for the inner halo is [Fe/H]$= -1.6$. The average metallicity this sample was [Fe/H]$= -1.8$. Because the SkyMapper telescope was searching for metal-poor halo stars, the fact that the average falls within the metallicity range for halo stars is quite significant.

Additionally, further analysis of these metal-poor stars can be done to learn more specifically about nucleosynthesis or star formation and death since the first generation of stars formed. Abundances of particular elements in the most metal-poor stars can be determined. From a comparison between iron abundance and abundances of other elements, patterns of element synthesis may be revealed.

6   Acknowledgments

References

[1] A. Frebel, N. Christlieb, J. E. Norris, C. Thom, T. C. Beers, and J. Rhee. Discovery of HE 1523-0901, a Strongly r-Process-enhanced Metal-poor Star with Detected Uranium. *ApJ*, 660:L117–L120, May 2007.

[2] T. C. Beers, G. W. Preston, and S. A. Shectman. A search for stars of very low metal abundance. I. *Astronomical Journal*, 90:2089–2102, Oct. 1985.

[3] T. C. Beers, G. W. Preston, and S. A. Shectman. A search for stars of very low metal abundance. II. *Astronomical Journal*, 103:1987–2034, June 1992.

[4] N. Christlieb, L. Wisotzki, D. Reimers, D. Homeier, D. Koester, and U. Heber. The stellar content of the Hamburg/ESO survey I. Automated selection of DA white dwarfs. *Astronomy & Astrophysics*, 366:898–912, Feb. 2001.

[5] A. Frebel, W. Aoki, N. Christlieb, N. Ando, M. Asplund, P. S. Barklem, T. C. Beers, K. Eriksson, C. Fechner, M. Y. Fujimoto, S. Honda, T. Kajino, T. Minezaki, K. Nomoto, J. E. Norris, S. G. Ryan, M. Takada-Hidai, S. Tsangarides, and Y. Yoshli. Nucleosynthetic Signatures in the First Stars. *Nature*, 434:871–873, 2005.

[6] S. C. Keller, B. P. Schmidt, M. S. Bessell, P. G. Conroy, P. Francis, A. Granlund, E. Kowald, A. P. Oates, T. Martin-Jones, T. Preston, P. Tisserand, A. Vaccarella, and M. F. Waterson. The SkyMapper Telescope and The Southern Sky Survey. *PASA*, 24:1–12, May 2007.

[7] R. Bernstein, S. A. Shectman, S. M. Gunnels, S. Mochnacki, and A. E. Athey. MIKE: A Double Echelle Spectrograph for the Magellan Telescopes at Las Campanas Observatory. In M. Iye and A. F. M. Moorwood, editors, *Society of Photo-Optical Instrumentation Engineers (SPIE) Conference Series*, volume 4841 of *Society of Photo-Optical Instrumentation Engineers (SPIE) Conference Series*, pages 1694–1704, Mar. 2003.

[8] C. A. Sneden. *Carbon and Nitrogen Abundances in Metal-Poor Stars.* PhD thesis, The University of Texas at Austin, 1973.

[9] J. P. Fulbright. Abundances and Kinematics of Field Halo and Disk Stars. I. Observational Data and Abundance Analysis. *The Astronomical Journal*, 120:1841–1852, Oct 2000.

[10] A. J. Cenarro, R. F. Peletier, P. Sánchez-Blázquez, S. O. Selam, E. Toloba, N. Cardiel, J. Falcón-Barroso, J. Gorgas, J. Jiménez-Vicente, and A. Vazdekis. Medium-resolution Isaac Newton Telescope library of empirical spectra - II. The stellar atmospheric parameters. *Monthly Notices of the Royal Astronomical Society*, 374:664–690, Jan. 2007.

[11] D. Carollo, T. C. Beers, Y. S. Lee, M. Chiba, J. E. Norris, R. Wilhelm, T. Sivarani, B. Marsteller, J. A. Munn, C. A. L. Bailer-Jones, P. R. Fiorentin, and D. G. York. Two stellar components in the halo of the Milky Way. *Nature*, 450:1020–1025, Dec. 2007.

[12] R. Cayrel, E. Depagne, M. Spite, V. Hill, F. Spite, P. François, B. Plez, T. Beers, F. Primas, J. Andersen, B. Barbuy, P. Bonifacio, P. Molaro, and B. Nordström. First stars V - Abundance patterns from C to Zn and supernova yields in the early Galaxy. *Astronomy & Astrophysics*, 416:1117–1138, Mar. 2004.

[13] A. Frebel and J. E. Norris. Metal-poor Stars and the Chemical Enrichment of the Universe. *Planets, Stars, and Stellar Systems*, 5, 2012.

[14] T. C. Beers and N. Christlieb. The Discovery and Analysis of Very Metal-Poor Stars in the Galaxy. *Annual Review of Astronomy and Astrophysics*, 43:531–580, 2005.

[15] A. Frebel. Metal-Poor Stars and the Rest of the Universe. Website: http://space.mit.edu/home/afrebel/theory.html.

A   Metallicities and Stellar Parameters

Obs. Date	Star Name	T_{eff}	$\log g$	[Fe/H]	v_{micro}
May 2012	1003-13-419	4900	2.0	−1.5	2.0
May 2012	1003-21-449	4900	2.0	−1.5	2.0
May 2012	1003-30-468	5100	2.5	−1.5	2.0
May 2012	1006-11-315	5700	3.5	−1.5	2.0
May 2012	1006-15-276	4900	2.0	−1.6	2.0
May 2012	1006-18-775	4900	2.0	−1.5	1.7
May 2012	1006-2-846	5400	3.2	−1.5	1.8
May 2012	1006-22-104	5300	3.0	−1.5	1.8
May 2012	1006-5-471	5200	2.8	−1.5	2.0
May 2012	1006-7-817	4900	2.0	−2.0	2.0
May 2012	1163-10-1432	4800	1.8	−2.7	2.0
May 2012	1163-27-65	5200	2.8	−1.5	2.3
May 2012	1163-29-4	5800	3.6	−0.1	2.0
May 2012	1163-29-572	5800	3.8	−1.5	2.3
May 2012	1163-32-174	5200	2.8	−1.5	2.0
May 2012	1163-4-1120	5000	2.1	−2.5	2.0
May 2012	1163-6-1332	5300	3.0	−2.4	2.0
May 2012	1163-6-1516	6300	3.9	−1.5	2.0
May 2012	1294-1-688	4700	1.6	−2.5	2.1
May 2012	1294-14-527	5000	2.1	−1.5	1.8
May 2012	1294-19-202	5100	2.5	−1.5	2.0
May 2012	1294-27-495	4600	1.6	−2.4	2.0
May 2012	1294-6-668	4600	1.6	−2.6	1.8
May 2012	1300-27-79	5400	3.2	−1.5	2.0
May 2012	1300-28-128	6600	4.5	−1.5	2.0
May 2012	1300-28-517	5200	2.8	−1.5	2.0
May 2012	1300-28-616	4500	1.4	−1.5	1.8
May 2012	1300-5-462	5800	3.6	−1.5	2.0
May 2012	1862-1-142	5100	2.6	−1.5	1.8
May 2012	1862-1-334	5600	3.4	−1.5	2.5
May 2012	2127-1-3912	4700	1.6	−1.5	2.0
May 2012	2127-10-1568	5400	3.2	−1.5	2.0
May 2012	2127-19-1247	5000	2.4	−1.5	2.0
May 2012	2127-2-1365	5100	2.5	−1.5	2.0
May 2012	2127-20-245	4800	1.8	−2.4	2.0
May 2012	2127-23-357	5100	2.5	−2.4	2.2
May 2012	2127-24-1381	4700	1.6	−2.5	2.2
May 2012	2127-3-571	6000	3.6	−0.1	2.0
May 2012	2127-31-1049	4900	2.0	−2.4	2.0
May 2012	2127-4-1321	4900	2.0	−1.5	1.8
May 2012	213-12-321	5900	3.6	−0.4	2.0
May 2012	213-12-996	6000	3.6	−1.5	2.2
May 2012	213-19-660	5800	3.6	−0.5	2.0
May 2012	213-19-682	5900	3.6	−1.5	2.0
May 2012	213-19-707	5700	3.5	−1.5	2.2
May 2012	213-29-490	6100	3.7	−1.5	2.3
May 2012	213-29-75	5900	3.6	−1.5	2.0
May 2012	213-6-630	6000	3.6	−1.5	2.0
May 2012	216-4-236	5100	2.5	−1.5	2.0
May 2012	368-28-4	6000	3.6	−1.5	2.0
May 2012	371-15-876	4900	2.0	−1.5	1.8
May 2012	371-2-247	5100	2.5	−1.5	2.0
May 2012	377-1-266	5700	3.5	−1.5	2.0
May 2012	377-1-96	6300	3.9	−1.5	2.0
May 2012	377-14-478	6100	3.9	−0.5	2.0
May 2012	377-14-577	6200	3.8	−1.5	2.0
May 2012	377-16-186	6600	4.0	−0.5	2.0
May 2012	377-16-767	5800	3.6	−1.5	2.0
May 2012	377-2-802	6200	3.9	−1.5	2.2
May 2012	377-2-950	5800	3.6	−1.5	2.0
May 2012	377-29-61	6200	3.8	−1.5	2.1
May 2012	377-3-166	5900	3.6	−1.5	2.0
May 2012	377-30-487	6100	3.9	−2.3	2.0
May 2012	377-31-473	6100	3.9	−1.5	2.0
May 2012	62-31-344	5100	2.5	−1.5	2.0
May 2012	62-4-702	5400	3.2	−1.5	2.2
May 2012	80-15-493	5400	3.2	−1.5	2.0
May 2012	80-26-231	5000	2.1	−1.5	2.0
May 2012	80-3-411	5100	2.5	−1.5	1.9
May 2012	80-30-290	5000	2.1	−2.2	2.0
May 2012	80-30-397	5200	2.6	−1.5	2.0
May 2012	80-9-505	5500	3.4	−1.5	1.8
May 2012	825-25-465	5500	3.4	−1.5	2.3
May 2012	825-9-1186	5900	3.6	−1.5	2.0
May 2012	95-15-32	5000	2.1	−1.5	2.0
May 2012	95-24-12	5200	2.7	−1.5	2.0
May 2012	95-26-473	5800	3.6	−0.1	2.0
May 2012	95-32-591	5300	3.0	−1.5	1.8
May 2012	95-4-495	4800	1.8	−1.5	2.2

Table 3: T_{eff}, $\log g$, v_{micro}, and [Fe/H] estimate for the final iteration for each star.

Obs. Date	Star Name	T_{eff}	$\log g$	[Fe/H]	v_{micro}
May 2012	997-15-614	4400	1.2	−2.5	2.0
May 2012	997-16-629	4800	1.8	−1.5	2.0
May 2012	997-16-678	4900	2.0	−1.5	2.0
May 2012	997-17-98	5600	3.4	−1.5	2.0
May 2012	997-19-448	5400	3.2	−1.5	2.4
May 2012	997-24-664	5300	3.0	−2.3	2.1
May 2012	997-28-81	4600	1.6	−1.5	2.0
May 2012	f01-233	5700	3.5	−1.5	2.3
May 2012	f01-91	5600	3.4	−1.5	2.0
May 2012	f02-205	5400	3.2	−1.5	2.2
May 2012	f02-339	5100	2.5	−2.9	2.0
May 2012	f03-106	6000	3.6	−2.4	2.4
May 2012	f03-183	6300	3.9	−1.5	2.2
May 2012	f03-68	5000	2.1	−3.1	2.5
May 2012	f04-338	5400	3.2	−2.5	2.0
May 2012	f09-206	5400	3.2	−1.5	2.0
May 2012	f09-384	5100	2.5	−2.5	2.0
May 2012	f09-80	4700	1.6	−2.8	2.2
May 2012	f10-358	6500	4.0	−1.5	2.1
May 2012	f11-23	5900	3.6	−1.5	2.0
Nov 2012	f121	5100	2.5	−2.3	2.0
Nov 2012	f181	5300	3.0	−2.4	2.1
Nov 2012	f278	5600	3.4	−1.5	2.0
Nov 2012	f280	5600	3.4	−2.3	2.0
Nov 2012	f280	5900	3.6	−1.5	2.0
Feb 2012	f3-1	5800	3.6	−0.8	2.3
Feb 2012	f3-11	5000	2.1	−1.7	2.3
Feb 2012	f3-12	5000	2.1	−2. 9	2.0
Feb 2012	f3-12	5400	3.2	−1.5	2.5
Feb 2012	f3-13	5200	2.8	−2.0	2.0
Feb 2012	f3-14	5300	3.0	−1.5	2.4
Feb 2012	f3-15	5100	2.5	−1.5	2.1
Feb 2012	f3-16	5300	3.0	−1.5	2.2
Feb 2012	f3-16	6100	3.9	−1.5	2.1
Feb 2012	f3-17	5600	3.4	−1.8	2.2
Feb 2012	f3-18	4700	1.6	−1.7	2.1
Feb 2012	f3-19	5800	3.6	−1.0	2.2
Feb 2012	f3-20	5300	3.0	−2.4	2.1
Feb 2012	f3-21	5100	2.5	−2.0	2.2
Feb 2012	f3-22	5100	2.5	−1.5	2.2
Feb 2012	f3-2comb	6200	3.8	−1.5	2.4
Feb 2012	f3-3	5600	3.4	−0.8	2.0
Feb 2012	f3-4	6000	3.6	−1.4	2.4
Feb 2012	f3-6	6000	3.6	−0.2	2.2
Feb 2012	f3-7	5900	3.7	−0.5	2.4
Feb 2012	f3-8	6000	3.6	−0.5	2.4
Feb 2012	f3-9	5400	3.2	−0.3	2.0
Nov 2012	f33-138	5600	3.4	−1.5	2.0
Nov 2012	f33-97	4900	2.0	−3.1	2.0
Nov 2012	f34-462	5400	3.2	−1.5	2.0
Nov 2012	f370	4900	2.0	−1.5	2.0
Feb 2012	f4-1	5200	2.8	−2.3	2.0
Feb 2012	f5-11	5800	3.6	−0.3	2.4
Feb 2012	f5-12	5300	3.0	−1.5	2.0
Feb 2012	f5-12	5400	3.2	−1.5	2.2
Feb 2012	f5-13	5900	3.7	−1.0	2.0
Feb 2012	f5-2	5700	3.5	−1.0	2.1
Feb 2012	f5-4	5800	3.6	−0.5	2.1
Feb 2012	f5-5	5900	3.7	−0.5	2.1
Feb 2012	f5-6	5100	2.5	−1.8	2.1
Feb 2012	f5-7	4900	2.0	−2.1	2.0
Feb 2012	f5-8	5900	3.7	−1.5	2.0
Feb 2012	f5-9	5000	2.0	−2.0	2.1
Feb 2012	f6-1	5900	3.7	−0.5	2.2
Feb 2012	f6-10	5200	2.8	−1.8	2.2
Feb 2012	f6-11	5100	2.5	−2.0	2.4
Feb 2012	f6-12	4800	1.8	−2.3	2.2
Feb 2012	f6-12	4800	1.8	−2.6	2.1
Feb 2012	f6-13	6500	4.0	−0.2	2.2
Feb 2012	f6-14	4700	1.6	−1.5	2.0
Feb 2012	f6-14	4800	1.8	−2.0	2.2
Feb 2012	f6-15	4600	1.4	−1.7	2.0
Feb 2012	f6-16	4800	1.8	−2.3	2.5
Feb 2012	f6-17	4600	1.4	−2.4	2.3
Feb 2012	f6-17	4700	1.6	−1.5	1.8
Feb 2012	f6-18	4700	1.6	−1.5	2.0
Feb 2012	f6-18	5100	2.4	−1.5	2.3
Feb 2012	f6-20	5200	2.8	−1.5	2.0
Feb 2012	f6-20	5300	3.0	−1.8	2.3
Feb 2012	f6-21	5200	2.8	−1.5	2.1
Feb 2012	f6-22	5300	3.0	−1.75	2.0
Feb 2012	f6-23	4900	2.0	−2.0	2.2
Feb 2012	f6-24	5300	3.0	−1.3	2.1
Feb 2012	f6-25	4800	1.8	−2.2	2.1
Feb 2012	f6-27	5200	2.8	−1.5	2.3

Obs. Date	Star Name	T_{eff}	$\log g$	[Fe/H]	v_{micro}
Feb 2012	f6-28	4400	3.6	-1.3	2.0
Feb 2012	f6-4	6200	3.8	-0.8	2.2
Feb 2012	f6-6	4800	1.8	-1.1	2.2
Feb 2012	f6-7	4600	1.6	-2.9	2.0
Feb 2012	f6-7	4900	2.0	-2.0	2.4
Feb 2012	f6-8	4700	1.6	-3.0	2.4
Feb 2012	f6-9	4500	1.4	-3.1	2.6
Feb 2012	f6-9	4300	1.0	-3.1	2.0
Feb 2012	f7-1	4400	1.2	-2.5	2.0
Feb 2012	f7-1	4500	1.4	-2.9	2.0
Feb 2012	f7-10	5200	2.8	-1.5	2.0
Feb 2012	f7-11	5800	3.6	-1.5	2.2
Feb 2012	f7-12	4900	2.0	-1.5	2.0
Feb 2012	f7-2	4900	2.0	-1.7	2.3
Feb 2012	f7-3	5000	2.1	-1.8	2.0
Feb 2012	f7-4	5000	2.1	-1.2	2.3
Feb 2012	f7-5	4900	2.0	-1.5	2.0
Feb 2012	f7-6	5000	2.1	-1.8	2.3
Feb 2012	f7-7	4700	1.0	-1.7	2.2
Feb 2012	f7-8	5000	2.0	-1.5	2.3
Feb 2012	f7-9	5200	2.8	-1.5	2.2
Nov 2012	f85	5200	2.8	-2.3	2.0
Nov 2012	f91	5300	3.0	-1.5	2.0
Nov 2012	f93	5200	2.8	-1.5	2.2
May 2012	hd74000	6100	3.9	-1.5	2.0
Feb 2012	he0556$-$5127	5000	2.1	-1.5	2.2
Feb 2012	he1300+0157	5200	2.8	-1.5	2.3
Feb 2012	he1506$-$0113	5000	2.1	-1.5	1.8

Star Name	Final [Fe/H]
f3-2comb	0.00
368-28-4	-0.02
213-19-707	-0.06
1163-29-4	-0.08
f3-6	-0.10
f6-13	-0.22
f3-8	-0.26
1300-5-462	-0.32
377-2-802	-0.34
2127-3-571	-0.35
377-31-473	-0.38
213-12-321	-0.40
213-12-996	-0.42
377-14-478	-0.42
f3-9	-0.42
825-9-1186	-0.43
f5-11	-0.45
377-16-186	-0.47
377-1-96	-0.47
95-26-473	-0.47
213-29-490	-0.50
f3-7	-0.51
1300-28-128	-0.53
f5-4	-0.56
f5-8	-0.57
213-19-660	-0.58
377-16-767	-0.59
f11-23	-0.61
f5-5	-0.62
f6-1	-0.62
377-14-577	-0.66
377-29-61	-0.66
f6-4	-0.73
377-3-166	-0.74
80-15-493	-0.76
997-17-98	-0.77
213-29-75	-0.80
1163-6-1516	-0.81
213-19-682	-0.82
f3-3	-0.83
f3-1	-0.87
f93	-0.89
f5-2	-0.89
213-6-630	-0.92
f3-19	-0.92
f3-14	-0.97
f6-6	-1.01
1163-29-572	-1.02
f6-27	-1.02

Star Name	[Fe/H]
1006-2-846	-1.05
f3-4	-1.05
f33-0825-138	-1.09
1006-11-315	-1.10
1006-22-104	-1.11
f34-0825-462	-1.12
377-1-266	-1.13
1163-27-65	-1.14
377-2-950	-1.16
997-16-678	-1.16
62-4-702	-1.19
2127-19-1247	-1.22
1300-28-517	-1.23
f7-4	-1.23
f6-28	-1.24
f7-9	-1.25
80-30-397	-1.29
f3-22	-1.30
f7-3	-1.30
f6-24	-1.33
f7-5	-1.34
f3-12	-1.35
1294-19-202	-1.36
377-30-487	-1.36
f7-6	-1.39
f5-13	-1.40
f7-2	-1.40
f7-8	-1.40
997-16-629	-1.42
f3-11	-1.44
f6-10	-1.44
1003-30-468	-1.45
f6-21	-1.46
f7-7	-1.46
2127-2-1365	-1.52
1006-18-775	-1.54
216-4-236	-1.54
1006-5-471	-1.56
1294-14-527	-1.57
f3-15	-1.57
f3-16	-1.57
f6-18	-1.57
1006-15-276	-1.58
80-3-411	-1.58
f3-13	-1.62
1163-32-174	-1.63
2127-4-1321	-1.64
371-15-876	-1.64
f6-15	-1.65
f7-10	-1.65
f6-20	-1.66
1862-1-142	-1.68
95-32-591	-1.71
2127-10-1568	-1.72
f03-183	-1.72
f3-18	-1.73
f6-14	-1.74
f5-6	-1.75
f6-20	-1.75
f6-22	-1.75
f7-12	-1.75
371-2-247	-1.76
80-26-231	-1.76
f3-21	-1.76
f5-12	-1.76
f10-358	-1.78
1003-13-419	-1.80
62-31-344	-1.80
95-24-12	-1.80
1003-21-449	-1.81
f6-11	-1.84
f3-17	-1.86
f5-9	-1.86
f6-14	-1.86
1300-27-79	-1.87
f7-11	-1.88
f6-25	-1.89
80-30-290	-1.92
f91	-1.92
1006-7-817	-1.95
997-19-448	-1.95
95-15-32	-1.98
f5-12	-2.00

1300-28-616	-2.02
1862-1-334	-2.02
f370	-2.04
f6-23	-2.04
f03-106	-2.07
997-28-81	-2.08
95-4-495	-2.10
f01-91	-2.10
f5-7	-2.10
f6-18	-2.11
f278	-2.12
80-9-505	-2.13
825-25-465	-2.13
f01-233	-2.14
f6-7	-2.15
2127-20-245	-2.21
2127-1-3912	-2.22
f02-205	-2.23
f6-12	-2.24
f4-1	-2.28
f121	-2.29
f6-16	-2.30
f6-17	-2.31
1294-1-688	-2.32
f6-12	-2.33
997-24-664	-2.38
f09-206	-2.40
2127-31-1049	-2.41
f3-20	-2.41
f6-17	-2.41
f7-1	-2.42
1294-27-495	-2.43
1163-10-1432	-2.44
2127-23-357	-2.44
f181	-2.45
f85	-2.49
997-15-614	-2.50
1163-4-1120	-2.51
1163-6-1332	-2.54
f280	-2.54
f6-9	-2.58
1294-6-668	-2.60
f7-1	-2.64
f09-384	-2.66
f04-338	-2.67
2127-24-1381	-2.75
f6-9	-2.79
f09-80	-2.80
f6-7	-2.91
f02-339	-2.93
f3-12	-2.96
f6-8	-2.96
f03-68	-2.97
f33-0825-97	-3.00
f3-16	-3.18

Table 4: Final [Fe/H] metallicities for all sample stars.